CHEMISTRY OF MATERIALS
Article

Chem. Mater. **2010,** *22,* 5333–5339 5333
DOI:10.1021/cm101663w

Controlled Synthesis of Sb Nanostructures and Their Conversion to $CoSb_3$ Nanoparticle Chains for Li-Ion Battery Electrodes

Jixin Zhu,[†] Ting Sun,[†] Junsong Chen,[‡] Wenhui Shi,[†] Xiaojun Zhang,[†] Xiongwen Lou,[‡] Subodh Mhaisalkar,[†,§] Huey Hoon Hng,[†] Freddy Boey,[†] Jan Ma,[†] and Qingyu Yan*[,†,§]

[†]*School of Materials Science and Engineering, Nanyang Technological University, 50 Nanyang Avenue, Singapore 639798,* [‡]*School of Chemical and Biomedical Engineering, Nanyang Technological University, 50 Nanyang Avenue, Singapore 639798, and* [§]*Energy Research Institute @ NTU, Nanyang Technological University, Singapore 637459*

Received June 15, 2010. Revised Manuscript Received August 2, 2010

Nanostructured Sb was prepared through a simple polyol process. Either Sb nanoparticles (Sb NP) or nanowires (Sb NW) were obtained by adjusting the concentration of surfactant. Electrochemical analyses revealed that the resultant Sb crystals displayed high charge storage capacities as Li-ion battery electrodes and relatively poor cycling retention during the charge−discharge process. For instance, the capacity was 560−584 mA h/g during the second cycle, which decreased to 120−200 mA h/g during the 70th cycle at a rate of 0.2 C. Thus, Sb NPs were reacted with Co precursors to form one-dimensional (1-D) NP chains wrapped in a polyvinyl pyridine layer, and the length of the NP chains could be adjusted by varying the concentration of polyvinyl pyridine. Through a controlled annealing process, the polyvinyl pyridine layer was converted to amorphous carbon, which led to the formation of 1-D core−shell structures with $CoSb_3$ NP chains entrapped in the carbon layer. Although $CoSb_3$ NP chains with a carbon shell displayed a lower initial charge storage capacity than Sb nanostructures, improved cycling performance was observed. The capacity was 468 mA h/g during the second cycle, which dropped to 421 mA h/g during the 70th cycle at a rate of 0.2 C. Compared to $CoSb_3$ produced via other techniques, $CoSb_3$/C NP chains displayed higher cycling stability, because of the presence of a carbon buffer layer.

Introduction

Rechargeable Li-ion batteries are the key to the development of portable electronic devices and hybrid electric vehicles; thus, technological improvements in Li-ion batteries are highly desirable.[1] The most common electrode materials in commercial Li-ion secondary batteries are graphite (anode) and $LiCoO_2$ (cathode). Although graphite electrodes display flat charge−discharge curves and excellent cyclability, the potential of lithium intercalation into graphite is not significantly greater than the deposition potential of metallic lithium. As a result, the dendritic growth of lithium metal can occur, which leads to shorts in the battery and safety issues.[1] Thus, alternative anode materials with improved safety and charge capacity are currently being investigated.

Sb and Sb alloys such as $CoSb_3$, ZnSb, Cu_2Sb, and SnSb have attracted considerable attention, because of their high Li storage capacities and more-positive Li intercalation voltages than that of graphite, which minimizes the risk of Li dendrite formation during fast recharge.[1−4] However, the lithiation process in Sb results in significant volume expansion (up to 150%), which leads to poor charge/discharge cycling performance.[5,6] Alloying Sb with another metal, such as Co, Zn, In, or Cu, can alleviate volume expansion.[7−11] Furthermore, by nanostructuring the electrode materials or forming a complex structure (coating nanocrystals with a carbon layer),[12] the tolerance to structural strains and the surface-to-volume ratio can be enhanced,

*Author to whom correspondence should be addressed. E-mail: alexyan@ntu.edu.sg.

(1) Tarascon, J. M.; Armand, M. *Nature* **2001**, *414*, 359–367.
(2) Mosby, J. M.; Prieto, A. L. *J. Am. Chem. Soc.* **2008**, *130*, 10656–10661.
(3) Li, H.; Wang, Q.; Shi, L. H.; Chen, L. Q.; Huang, X. J. *Chem. Mater.* **2002**, *14*, 103–108.
(4) Kim, H.; Cho, J. *Chem. Mater.* **2008**, *20*, 1679–1681.
(5) Chen, W. X.; Lee, J. Y.; Liu, Z. L. *Carbon* **2003**, *41*, 959–966.
(6) Bryngelsson, H.; Eskhult, J.; Nyholm, L.; Herranen, M.; Alm, O. *Chem. Mater.* **2007**, *19*, 1170–1180.
(7) Sarakonsri, I.; Johnson, C. S.; Hackney, S. A.; Thackeray, M. M. *J. Power Sources* **2006**, *153*, 319–327.
(8) Zhao, H. L.; Yin, C. L.; Guo, H.; He, H. C.; Qiu, W. H.; Li, Y. *J. Power Sources* **2007**, *174*, 916–920.
(9) Xie, H.; Cao, G. S.; Zhong, Y. D.; Zhao, X. B. *J. Electroanal. Chem.* **2004**, *568*, 323–327.
(10) Stjerndahl, M.; Bryngelsson, H.; Gustafsson, T.; Vaughey, J. T.; Thackeray, M. M.; Edstrom, K. *Electrochim. Acta* **2007**, *52*, 4947–4955.
(11) Song, S. W.; Reade, R. P.; Cairns, E. J.; Vaughey, J. T.; Thackeray, M. M.; Striebel, K. A. *J. Electrochem. Soc.* **2004**, *151*, A1012–A1019.
(12) Lou, X. W.; Li, C. M.; Archer, L. A. *Adv. Mater.* **2009**, *21*, 2536–2539.

Published on Web 08/16/2010

which improves the cyclability and increases the specific charge capacity of the material.[13−15] Thus, a synthetic strategy for the production of Sb and Sb alloy nanocrystals with a controlled size, morphology, and composition must be developed to obtain superior anode materials for Li-ion batteries.

Many different processes for the fabrication of nanocrystals have been developed, including hard template methods,[12] virus-based template methods[16,17] and vapor−liquid−solid processes.[14] Solvothermal/hydrothermal techniques[18−20] are attractive, because they are highly flexible and can be easily adapted for large-scale production. However, a controlled solvothermal/hydrothermal synthesis of Sb and Sb-based alloy nanocrystals remains a significant challenge, because of the lack of suitable surfactants that interact effectively with Sb. Sb displays high diffusivity and low surface energy;[21,22] thus, during nanocrystal growth, Sb can easily diffuse onto the surface of the material and reduce the total surface energy, as demonstrated in the molecular beam epitaxial growth process.[23] Without effective functional groups to inhibit growth, the particle size and uniformity of the material is difficult to control, and agglomeration can occur.

In the present study, a new solvothermal approach was developed to obtain Sb nanocrystals with adjustable morphology. With the proposed methodology, nanoparticles (denoted hereafter as NPs) or nanowires (denoted hereafter as NWs) could be obtained by tuning various parameters. The results of electrochemical tests revealed that the resultant Sb nanocrystals exhibited high charge storage capacities as Li-ion battery anodes and relatively poor cycling retention during the charge−discharge process. The Sb nanoparticles were further reacted with $CoCl_2 \cdot 6H_2O$ to form one-dimensional (1-D) NP chains with tunable lengths, which were enwrapped in a polyvinyl pyridine (PVP) layer. After annealing at 500 °C under vacuum, the PVP layer was converted to amorphous carbon, which led to the formation of 1-D core−shell structures with $CoSb_3$ NP chains entrapped in the carbon layer. Although encapsulated $CoSb_3$ NP chains showed lower initial charge capacities than pure Sb nanocrystals, improved cycling charge−discharge performance was observed, and a capacity of 421 mA h/g was attained after 70 cycles at a rate of 0.2 C. Compared to $CoSb_3$ produced via other techniques,[9,24,25] NP chains also exhibited higher cyclability; thus, the proposed synthetic approach is a useful route for the preparation of Sb-based alloy nanostructures for various electronic applications.

Experimental Section

Synthesis of Sb NPs/Sb NWs. To synthesize Sb nanoparticles (Sb NPs), 1 mmol of $SbCl_3 \cdot 6H_2O$ and 0.1 g of PVP (0.5 g of PVP for the preparation of Sb nanowires (Sb NWs)) were dissolved in 35 mL of 1,5-pentanediol. To the resulting solution, a mixture of 2 mmol of $NaBH_4$ in 10 mL of 1,5-pentanediol at 140 °C was injected at 180 °C. The mixture was maintained at 180 °C for 3 min under an Ar atmosphere. Upon completion, the samples were washed by centrifugation and were dispersed in 10 mL of ethanol. To test the materials in Li-ion batteries, the samples were annealed at 400 °C for 30 min under an Ar atmosphere.

Conversion of Sb NPs to Nanochains. To convert Sb NPs to nanochains, 0.15 mmol of Sb NPs, 0.2 g of PVP, and 0.1 mmol of $CoCl_2 \cdot 6H_2O$ were added to 25 mL of 1,5-pentanediol, and the resulting solution was maintained at 140 °C for 10 min. Next, the temperature was increased to 240 °C, and a mixture of 0.5 mmol of $NaBH_4$ in 5 mL of 1,5-pentanediol was added into the solution. The resulting suspension was maintained at 240 °C for 60 min under an Ar atmosphere. The samples were washed by centrifugation and were dispersed in 10 mL of ethanol. The samples were annealed in a vacuum furnace at 500 °C and $(2-3) \times 10^{-6}$ Torr for 60 min. At a Sb NP:$CoCl_2 \cdot 6H_2O$ molar ratio of 1.5, the annealed products existed primarily as a $CoSb_3$ phase.

One-Step Synthesis of a Sb/CoSb Mixture. To prepare a mixture of Sb/CoSb, 0.15 mmol of $SbCl_3$, 0.1 of mmol $CoCl_2 \cdot 6H_2O$, and 0.2 g of PVP were added to 25 mL of 1,5-pentanediol, and the resulting solution was maintained at 140 °C for 10 min. Next, a mixture of 1 mmol of $NaBH_4$ in 5 mL of 1,5-pentanediol was injected at 240 °C, and the resulting suspension was maintained at 240 °C for 60 min under an Ar atmosphere.

Characterization. The morphology of the samples was investigated with a field-emission scanning electron microscopy (SEM) system (JEOL, Model JSM-6340F), and the nanostructures of the materials were characterized with a transmission electron microscopy (TEM) system (JEOL, Model JEM-2010) operating at 200 kV. To observe the samples via TEM, a suspension of the material was deposited dropwise onto carbon-coated copper grids

(13) Chen, J.; Cheng, F. Y. *Acc. Chem. Res.* **2009**, *42*, 713–723.
(14) Cui, L. F.; Yang, Y.; Hsu, C. M.; Cui, Y. *Nano Lett.* **2009**, *9*, 3370–3374.
(15) Hassoun, J.; Derrien, G.; Panero, S.; Scrosati, B. *Adv. Mater.* **2008**, *20*, 3169–3175.
(16) Nam, K. T.; Kim, D. W.; Yoo, P. J.; Chiang, C. Y.; Meethong, N.; Hammond, P. T.; Chiang, Y. M.; Belcher, A. M. *Science* **2006**, *312*, 885–888.
(17) Mao, C. B.; Solis, D. J.; Reiss, B. D.; Kottmann, S. T.; Sweeney, R. Y.; Hayhurst, A.; Georgiou, G.; Iverson, B.; Belcher, A. M. *Science* **2004**, *303*, 213–217.
(18) Purkayastha, A.; Yan, Q. Y.; Gandhi, D. D.; Li, H. F.; Pattanaik, G.; Borca-Tasciuc, T.; Ravishankar, N.; Ramanath, G. *Chem. Mater.* **2008**, *20*, 4791–4793.
(19) Yan, Q. Y.; Raghuveer, M. S.; Li, H. F.; Singh, B.; Kim, T.; Shima, M.; Bose, A.; Ramanath, G. *Adv. Mater.* **2007**, *19*, 4358–4363.
(20) Zhu, J. X.; Sun, T.; Hng, H. H.; Ma, J.; Boey, F. Y. C.; Lou, X. W.; Zhang, H.; Xue, C.; Chen, H. Y.; Yan, Q. Y. *Chem. Mater.* **2009**, *21*, 3848–3852.
(21) Yan, Q. Y.; Kim, T.; Purkayastha, A.; Ganesan, P. G.; Shima, M.; Ramanath, G. *Adv. Mater.* **2005**, *17*, 2233–2237.
(22) Yan, Q. Y.; Kim, T.; Purkayastha, A.; Xu, Y.; Shima, M.; Gambino, R. J.; Ramanath, G. *J. Appl. Phys.* **2006**, *99*, 08N709.
(23) Portavoce, A.; Gas, P.; Berbezier, I.; Ronda, A.; Christensen, J. S.; Kuznetsov, A. Y.; Svensson, B. G. *Phys. Rev. B* **2004**, *69*, 155415.
(24) Purkayastha, A.; Yan, Q. Y.; Raghuveer, M. S.; Gandhi, D. D.; Li, H. F.; Liu, Z. W.; Ramanujan, R. V.; Borca-Tasciuc, T.; Ramanath, G. *Adv. Mater.* **2008**, *20*, 2679–2684.
(25) Hao, E. C.; Lian, T. Q. *Chem. Mater.* **2000**, *12*, 3392–3396.

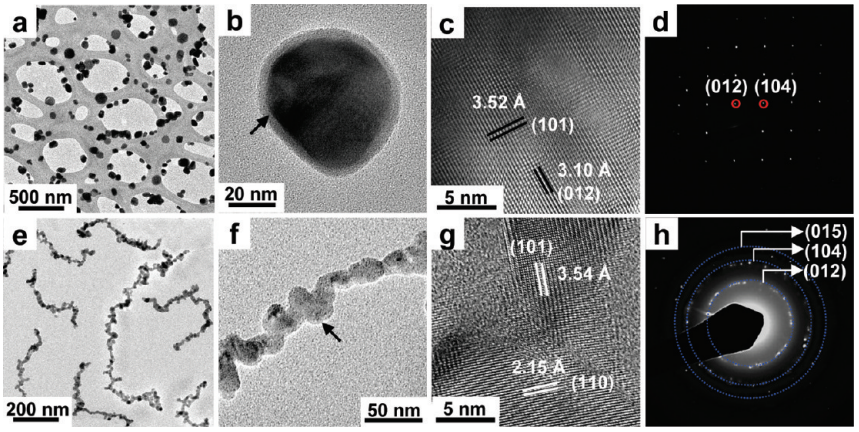

Figure 1. (a) Low-magnification TEM image of as-prepared Sb nanoparticles; (b) high-magnification TEM image of as-prepared Sb nanoparticles; (c) HRTEM image of a Sb nanoparticle and (d) the corresponding SAED pattern. (e) Low-magnification TEM images of as-prepared Sb nanowires; (f) high-magnification TEM images of as-prepared Sb nanowires; (g) HRTEM image of a segment of a Sb nanowires and (h) the corresponding SAED pattern. The arrows in panels (b) and (f) indicate the capping layer on the surface of Sb nanocrystals.

and dried at room temperature. Crystal phases were identified using a Scintag PAD-V X-ray diffractometer with Cu Kα irradiation, and Raman spectra were obtained with a WITec CRM200 confocal Raman microscopy system with a laser wavelength of 488 nm and a spot size of 0.5 mm. To calibrate the wavenumber, the Si peak at 520 cm^{-1} was used as a reference. IR spectra were obtained with a Fourier transform infrared spectrometer (Perkin−Elmer) that was equipped with a DGTS detector and a ZnSe window.

Electrochemical Measurements. Electrochemical measurements were conducted at room temperature, using two-electrode Swagelok cells with pure lithium metal as both the counter electrode and the reference electrode. The working electrode consisted of the active material (e.g., Sb NPs), a conductive agent (carbon black, Super P−Li) and a polymer binder [poly(vinylidene difluoride), PVDF, Aldrich] in a 70:20:10 ratio (by weight). The electrolyte consisted of 1.0 M $LiPF_6$ in a 50:50 wt:wt solution of ethylene carbonate and diethyl carbonate. The cell was assembled in an Ar-filled glovebox with moisture and oxygen concentrations of <1.0 ppm. The charge/discharge tests were performed with a NEWARE battery tester at a current density of 120 mA/g (0.2 C) and a voltage window of 0.01−1.5 V.

Results and Discussion

Bright-field TEM images (see Figures 1a and 1b) revealed that the Sb NPs were faceted, indicating that the NPs were crystalline. The Sb NPs displayed an average particle size of ~50 nm and a medium size distribution (see Figure S1 in the Supporting Information). High-resolution transmission electron microscopy (HRTEM) images revealed the presence of well-resolved atomic lattice planes, which indicated that single-crystalline Sb formed under the reaction conditions (see Figure 1c). The selected-area electron diffraction (SAED) pattern (see Figure 1d) clearly displayed a spot pattern corresponding to rhombohedral Sb (JCPD File Card No. 85-1322). Moreover, the results indicated that the formation of Sb NWs (see Figures 1e and 1f) with an average diameter of 30 nm could be achieved by increasing the concentration of PVP from 2.2 g/L to 11.1 g/L. The Sb nanowires produced in this study were distorted and slightly branched; thus, the exact length of the NWs could not be determined. The HRTEM image of Sb NWs revealed that the material possessed a polycrystalline structure (see Figure 1g), and the SAED results (see Figure 1h) displayed a ring pattern, which confirmed the formation of polycrystalline rhombohedral Sb (JCPD File Card No. 85-1322). Although materials with a rhombohedral crystal structure such as Bi_2Te_3[25] have a tendency to grow into 1-D nanostructures, the polycrystalline nature of the Sb NWs indicated that the growth of NWs was not closely related to the crystal structure of Sb. Alternatively, NW growth was attributed to the interaction between Sb seeds and PVP molecules. Normally, the adhesion of PVP onto different crystallographic facets of a crystal lattice is highly variable.[26,27] As Sb seeds form, their surfaces may become passivated; however, the ends of the seeds remain accessible to newly generated Sb atoms, which induces anisotropic growth, forming NWs. On Sb NPs and Sb NWs, a capping layer with a thickness of 5−12 nm was clearly observed. Fourier transform infrared (FTIR) spectra of the NPs revealed the presence of a Ni−C═O

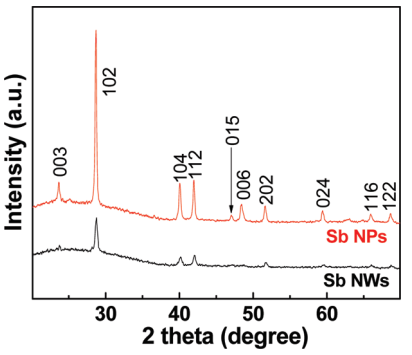

Figure 2. XRD patterns of as-prepared Sb nanoparticles and nanowires.

(26) Borodko, Y.; Habas, S. E.; Koebel, M.; Yang, P. D.; Frei, H.; Somorjai, G. A. *J. Phys. Chem. B* **2006**, *110*, 23052–23059.
(27) Ferrari, A. C.; Robertson, J. *Phys. Rev. B* **2001**, *64*, 075414.

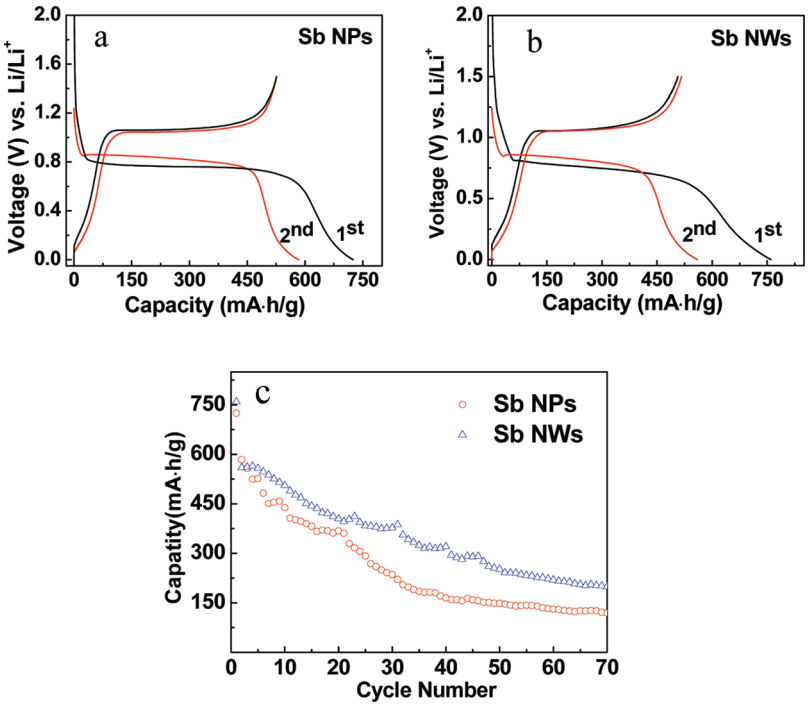

Figure 3. Charge−discharge curves of (a) Sb NPs and (b) Sb NWs for first and second cycles at a current density of 120 mA/g (0.2 C); (c) the cycling performance of (○) Sb NPs and (△) Sb NWs with a voltage window of 0.01−1.5 V and a current density of 120 mA/g (for a rate of 0.2 C).

stretching band at 679.7 cm^{-1} (see Figure S2 in the Supporting Information), which confirmed that PVP adhered to the material.[26,27] Thus, the capping layers on Sb nanocrystals were ascribed to PVP.

The XRD results (see Figure 2) revealed that impurity phases were not detected in Sb NPs and Sb NWs; however, a rhombohedral Sb phase was observed (JCPD File Card No. 85-1322). By analyzing the peak width of the XRD patterns using Scherrer's equation, the crystallites of Sb NPs and Sb NWs were estimated to be 50 and 22 nm, respectively, and the results were consistent with TEM and HRTEM observations (see Figure 1).

To test the materials in lithium ions batteries, the samples were annealed at 400 °C for 30 min under an Ar atmosphere. Although Sb nanocrystals did not show obvious agglomeration due to the presence of a surface capping layer (see Figure S3 in the Supporting Information), the D (1345 cm^{-1}) and G (1589 cm^{-1}) peaks of the Raman spectra (see Figure S4 in the Supporting Information) indicated the formation of amorphous carbon,[28] which was attributed to the carbonization of PVP. In some cases, a carbon layer has been shown to improve the functional properties of the core materials.[9] To study the Li-ion storage capabilities of annealed Sb NPs and NWs, a series of electrochemical measurements were carried out. The charge−discharge voltage profiles of the materials were obtained at a current density of 120 mA/g (0.2 C), and the results indicated that Sb nanocrystals displayed a distinct plateau at ~0.75 V (see Figures 3a and 3b), which was attributed to the alloying process of Sb and Li. Moreover, the charge−discharge voltage profiles revealed that the discharge capacities of Sb NWs and Sb NPs were 760 and 725 mA h/g, respectively. Similar patterns were observed during the subsequent charge process, and capacities of 507 and 526 mA h/g were obtained for Sb NWs and Sb NPs, respectively. As a result, the Coulombic efficiency of NWs and NPs was ~66.7% and ~72.6%, respectively. The high initial discharge capacities of Sb NWs and Sb NPs are closely related to irreversible reactions,[29,30] which result in relatively low first-cycle Coulombic efficiencies. A lower discharge capacity of 560 mA h/g and a corresponding charge capacity of 516 mA h/g were obtained for Sb NWs in the second cycle, yielding a Coulombic efficiency of 92.1%. Moreover, at a slightly lower charge/discharge capacity, the Coulombic efficiency of Sb NPs increased to 90.1% in the second cycle.

Figure 3c depicts the performance of Sb NWs and Sb NPs after 70 cycles. Both samples displayed large capacity losses during the charge−discharge process, although Sb NWs exhibited a higher capacity than Sb NPs. Specifically, the capacities of Sb NWs and Sb NPs decreased to 200 and 120 mA h/g, respectively, after 70 cycles. The higher Li storage capacity of Sb NWs was attributed to its smaller crystallite size, which allows a more-efficient diffusion of Li ions.[13] Moreover, the significant capacity loss during the cycling of both samples was ascribed to the large structural strain generated during the lithiation process.[31]

(28) Poizot, P.; Laruelle, S.; Grugeon, S.; Dupont, L.; Tarascon, J. M. *Nature* **2000**, *407*, 496–499.

(29) Lou, X. W.; Wang, Y.; Yuan, C. L.; Lee, J. Y.; Archer, L. A. *Adv. Mater.* **2006**, *18*, 2325–2329.

(30) Besenhard, J. O.; Wachtler, M.; Winter, M.; Andreaus, R.; Rom, I.; Sitte, W. *J. Power Sources* **1999**, *81*, 268–272.

(31) Johnson, C. S.; Vaughey, J. T.; Thackeray, M. M.; Sarakonsri, T.; Hackney, S. A.; Fransson, L.; Edstrom, K.; Thomas, J. O. *Electrochem. Commun.* **2000**, *2*, 595–600.

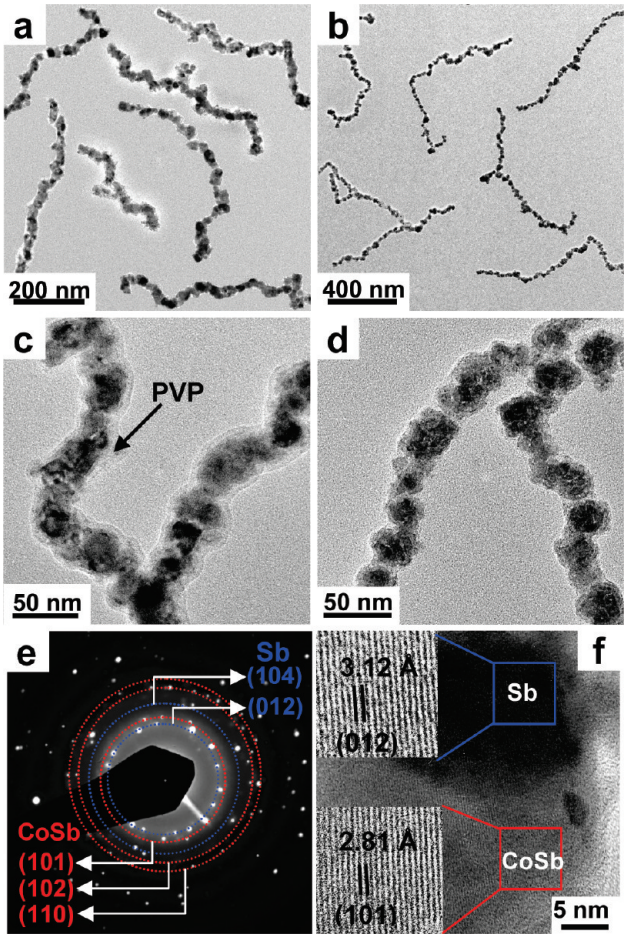

Figure 4. Low-magnification TEM images of as-prepared binary-phase Sb/CoSb NP chains obtained with (a) $X_{PVP\text{-}Sb} = 30$ and (b) $X_{PVP\text{-}Sb} = 6$, and the corresponding high-magnification TEM images Sb/CoSb NP chains obtained with (c) $X_{PVP\text{-}Sb} = 30$ and (d) $X_{PVP\text{-}Sb} = 6$, respectively. (e) SAED pattern of an as-prepared Sb/CoSb nanoparticle chain with $X_{PVP\text{-}Sb} = 6$, and (f) the corresponding HRTEM image.

Alloying Sb with other metallic elements may reduce volume expansion during the lithiation process;[11,32,33] thus, Sb NPs were reacted with $CoCl_2 \cdot 6H_2O$ to form NP chains (see Figure 4). The diameter of the NP chains was comparable to that of Sb NPs (50 nm), and the length of the NP chains could be tuned by adjusting the initial concentration of PVP. For example, at a PVP-to-Sb molar ratio ($X_{PVP\text{-}Sb}$) of 30 (see Figure 4a), the length of the NP chains was in the range of 500−600 nm. However, by decreasing $X_{PVP\text{-}Sb}$ to 6, the chain length increased to 0.9−1.5 μm (see Figure 4b). High-magnification TEM images indicated that the particle chains were entrapped inside a layer of PVP, and the thickness of the PVP layer depended on the initial concentration of PVP. For instance, the PVP layer of short chains was ~10 nm at $X_{PVP\text{-}Sb} = 30$ (see Figure 4c), and the PVP layer of long chains was ~4 nm at $X_{PVP\text{-}Sb} = 6$ (see Figure 4d).

(32) Vaughey, J. T.; Johnson, C. S.; Kropf, A. J.; Benedek, R.; Thackeray, M. M.; Tostmann, H.; Sarakonsri, T.; Hackney, S.; Fransson, L.; Edstrom, K.; Thomas, J. O. *J. Power Sources* **2001**, *97*−*8*, 194–197.
(33) Lu, Y. F.; Ganguli, R.; Drewien, C. A.; Anderson, M. T.; Brinker, C. J.; Gong, W. L.; Guo, Y. X.; Soyez, H.; Dunn, B.; Huang, M. H.; Zink, J. I. *Nature* **1997**, *389*, 364–368.

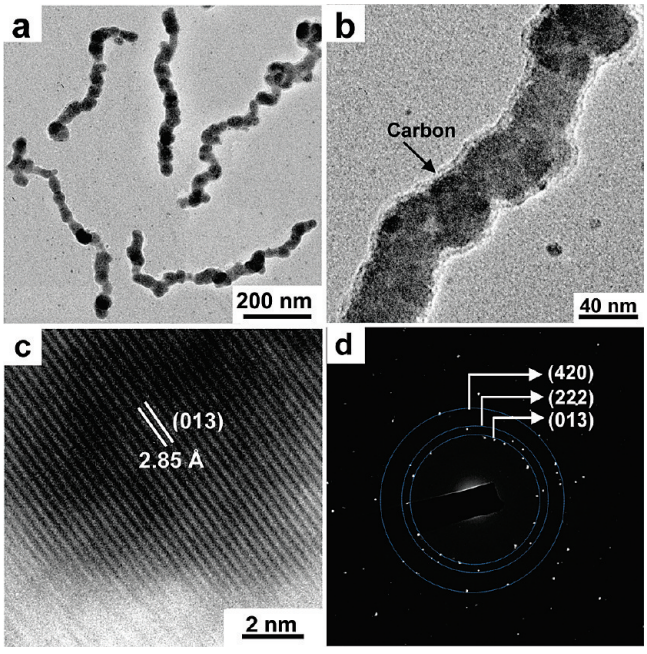

Figure 5. (a, b) Low-magnification TEM image of $CoSb_3$ NP chains obtained after annealing the binary-phase Co/CoSb nanoparticle chains with $X_{Sb-Co} = 1.5$ under vacuum at 500 °C for 60 min. (b) High-magnification TEM image of $CoSb_3$ NP chains obtained after annealing the binary-phased Co/CoSb nanoparticle chains with $X_{Sb-Co} = 1.5$ under vacuum at 500 °C for 60 min. (c) HRTEM image of the as-obtained $CoSb_3$ NP chain. (d) SAED pattern obtained from the $CoSb_3$ NP chains.

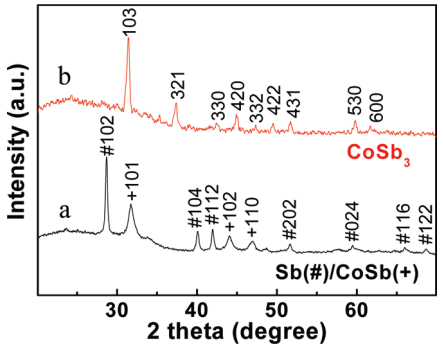

Figure 6. XRD patterns of (a) as-prepared binary-phase Sb(symbol: #)/CoSb (symbol: +) nanoparticle chains and (b) $CoSb_3$ nanoparticle chains obtained after annealing the Sb/CoSb chains with $X_{Sb-Co} = 1.5$ under vacuum at 500 °C for 60 min.

The SAED of the NP chain exhibited ring patterns (see Figure 4e), which were correlated to the diffraction of Sb and CoSb phases. HRTEM observations confirmed the coexistence of Sb crystals and CoSb crystals in the NP chains (see Figure 4f); however, the exact distribution of both phases was not well-defined. Thus, the synthesis conditions were varied to understand the formation of binary-phased Sb/CoSb NP chains. By replacing Sb NPs with NWs (see Figures 1e and 1f) in the aforementioned synthesis, agglomerated network structures were obtained (see Figure S5 in the Supporting Information). For comparison, a one-step synthesis was also conducted, yielding agglomerated clusters of Sb and CoSb with poorly defined morphology (see Figures S6a and S6b in the Supporting Information). Based on the aforementioned observations,

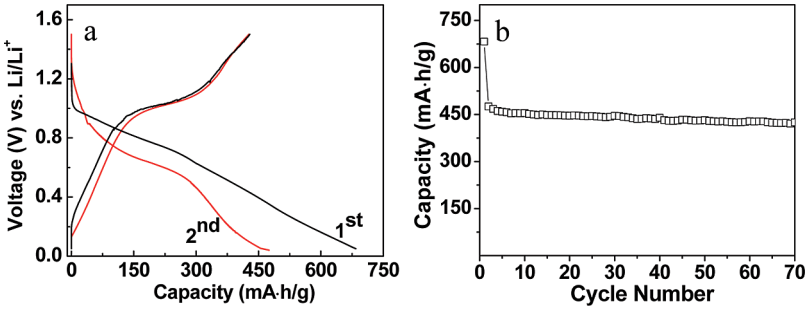

Figure 7. (a) Charge−discharge curves of the $CoSb_3$/C NP chains for first and second cycles at a current density of 120 mA/g (0.2 C). (b) Cycling performance of the $CoSb_3$/C NP chains with a voltage window of 0.01−1.5 V and a current density of 120 mA/g (0.2 C).

the formation of NP chains may be related to the assembly and connection of Sb NPs within the soft template, which is formed by PVP during the reaction with the Co precursor. The shape of the soft template in solution is typically related to the concentration of the surfactants.[34] As previously discussed, increasing the PVP concentration during the synthesis of Sb nanocrystals leads to the growth of NWs, which indicates that channel-shaped soft templates were formed in solution. In the second step, extra PVP was added along with the Co precursor to protect the products from agglomeration. As a result, channel-shaped micelles[35] may have formed, which assisted in particle chain formation.[36,37]

Annealing the NP chains under vacuum did not cause obvious changes to their morphology, as revealed by TEM analysis (see Figures 5a and 5b). The FTIR spectra of annealed NP chains did not display a N−C═O stretching band (see Figure S7 in the Supporting Information), and the Raman shift spectrum indicated the formation of amorphous carbon, which is similar to the results obtained from annealed Sb nanocrystals (see Figure S8 in the Supporting Information). The aforementioned results suggested that the PVP layers were transformed to amorphous carbon (see Figure 5b). These results suggest that the PVP layers change to amorphous carbon. Moreover, the annealing process also converts binary-phased NP chains into single-phased $CoSb_x$. Here, the value of x is determined by the molar ratio (X_{Sb-Co}) of Sb:$CoCl_2 \cdot 6H_2O$ during the second step of the synthesis. For instance, at a X_{Sb-Co} value of 1.5, single-phased $CoSb_3$ was obtained after annealing, as indicated by HRTEM and SAED (see Figures 5c and 5d). The HRTEM image of annealed $CoSb_3$ NP chains indicated that the material possessed a body-centered-cubic (bcc) structure (JCPD File Card No. 79-0976); however, the boundaries of the particles in the chains were indistinct. The ring patterns observed in the SAED pattern of the $CoSb_3$ chain confirmed the polycrystalline nature of the material.

The transition from binary phase to single phase, which is induced by vacuum annealing, was also confirmed by XRD (see Figure 6). The results revealed that the NP chains were composed of a Sb phase (JCPD File Card No. 85-1322) and CoSb phase (JCPD File Card No. 89-4867), which is consistent with the HRTEM and SAED results (see Figure 5e and 5f). Impurity phases were not detected, and the width of the CoSb peaks was broader than that of the Sb peaks, which suggested that CoSb crystals were smaller than Sb crystals. The XRD pattern of annealed samples with $X_{Sb-Co} = 1.5$ displayed peaks corresponding to a bcc $CoSb_3$ (JCPD File Card No. 79-0976) phase, which is in good agreement with HRTEM observations (see Figure 5c).

The lithium storage capacity of $CoSb_3$/C NP chains was evaluated using a two-electrode cell. A pair of cathodic and anodic peaks was observed in the cyclic voltammogram (CV) of the NP chains, from 0.01 to 1.5 V versus Li^+/Li at a scan rate of 0.5 mV/s (see Figure S9 in the Supporting Information). The aforementioned peaks were attributed to the following Li alloying and dealloying processes:[38] $Li_3Sb \leftrightarrow Sb_3Li^+ + 3e^-$. The cathodic peak was not readily apparent in the first discharge curve, which may be due to the sluggish kinetics of the first lithiation process.[38]

The charge−discharge voltage profiles (see Figure 7a) of the $CoSb_3$/C NP chains displayed a plateau at ~0.63 V in the second discharge curve at a current density of 120 mA/g (0.2 C); however, a plateau was not readily apparent in the first discharge curve. The presence of the plateau was attributed to the restructuring of $CoSb_3$ in the electrode system.[38,39] The NP chains displayed an initial discharge capacity of 680 mA h/g, which was 19.5% higher than the theoretical capacity of bulk $CoSb_3$ (569 mA h/g).[9] A capacity of 428 mA h/g was observed during the initial charging process, and a Coulombic efficiency of 63% was obtained. Irreversible capacity loss is often related to reactions of the electrolyte solution and the formation of a solid electrolyte interface (SEI) layer.[40] A lower discharge capacity of 468 mA h/g and a corresponding charge capacity of 426 mA h/g were obtained in the second cycle, leading to a Coulombic efficiency of 91%.

Although the capacity of $CoSb_3$/C NP chains was lower than that of pure Sb nanocrystals during the first 20

(34) Pileni, M. P. *Nat. Mater.* **2003**, *2*, 145–150.
(35) Wei, Y. H.; Tong, W. J.; Zimmt, M. B. *J. Am. Chem. Soc.* **2008**, *130*, 3399–3405.
(36) Wang, Y. L.; Jiang, X. C.; Herricks, T.; Xia, Y. N. *J. Phys. Chem. B* **2004**, *108*, 8631–8640.
(37) Xie, J.; Zhao, X. B.; Cao, G. S.; Zhao, M. J.; Su, S. F. *J. Power Sources* **2005**, *140*, 350–354.
(38) Alcantara, R.; Fernandez-Madrigal, F. J.; Lavela, P.; Tirado, J. L.; Jumas, J. C.; Olivier-Fourcade, J. *J. Mater. Chem.* **1999**, *9*, 2517–2521.
(39) Aurbach, D.; Eineli, Y.; Markovsky, B.; Zaban, A.; Luski, S.; Carmeli, Y.; Yamin, H. *J. Electrochem. Soc.* **1995**, *142*, 2882–2890.
(40) Park, C. M.; Sohn, H. J. *Adv. Mater.* **2009**, *22*, 47–52.

cycles, the cycling performance of NP chains was better (see Figure 7b). For instance, the capacity of the NP chains decreased from 468 mA h/g during the second cycle to 421 mA h/g after 70 cycles. Moreover, the theoretical capacity of $CoSb_3$ is 569 mA h/g, which is lower than that of pure Sb (660 mA h/g).[38] Compared to $CoSb_3$ obtained through other techniques,[9,24,25] $CoSb_3$/C NP chains produced in this study displayed superior cycling performance, because of their nanosized features and the presence of a carbon buffer layer.[12] The capacity of the NP chains after 70 cycles was slightly higher than that of graphite anodes.[1] Moreover, considering the need for safer operation of Li-ion batteries, the $CoSb_3$/C NP chains produced in this investigation are attractive anode materials.

Conclusion

In summary, we demonstrated that a simple solvothermal process can be used to prepare Sb nanocrystals with controlled morphology, including nanoparticles (NPs) or nanowires (NWs). The resulting Sb nanocrystals displayed high charge storage capacities and relatively poor cycling performance. The materials were tested as Li-ion battery electrodes, and a capacity of 120−200 mA h/g after 70 cycles was obtained. Binary-phase Sb/CoSb NP chains were produced via a second growth process by reacting Sb NPs with $CoCl_2 \cdot 6H_2O$. The results indicated that the length of the NP chains can be tuned by varying the initial concentration of PVP. $CoSb_3$ NP chains in a carbon shell were obtained after annealing the Sb/CoSb NP chains at a proper X_{Sb-Co} ratio. The $CoSb_3$/C NP chains displayed superior cycling stability, compared to pure Sb nanocrystals, and delivered a capacity of 421 mA h/g after 70 cycles. The proposed synthetic approach can also be used to prepare other useful Sb-based alloy nanostructures with specific sizes, morphologies, and compositions, including Cu_2Sb and Zn_4Sb_3, which can be used in applications such as Li-ion batteries and thermoelectric devices.

Acknowledgment. The authors gratefully acknowledge AcRF Tier 1 RG 31/08 of MOE (Singapore) and NRF2009EWT-CERP001-026 (Singapore).

Supporting Information Available: The morphology of annealed Sb nanocrystals, Raman shift spectra, FTIR spectra, sample morphology, and CV curves of NP chains. This material is available free of charge via the Internet at http://pubs.acs.org.